Behavior of Double-Hemisphere Thermohaline Flows in a Single Basin

BARRY A. KLINGER

Oceanographic Center, Nova Southeastern University, Dania Beach, Florida

JOCHEM MAROTZKE

Center for Global Change Science, Massachusetts Institute of Technology, Cambridge, Massachusetts

(Manuscript received 26 May 1997, in final form 12 March 1998)

ABSTRACT

A coarse resolution, three-dimensional numerical model is used to study how external parameters control the existence and strength of equatorially asymmetric thermohaline overturning in a large-scale, rotating ocean basin. Initially, the meridional surface density gradient is directly set to be larger in a ''dominant'' hemisphere than in a ''subordinate'' hemisphere. The two-hemisphere system has a broader thermocline and weaker upwelling than the same model with the dominant hemisphere only. This behavior is in accord with classical scaling arguments, providing that the continuity equation is employed, rather than the linear vorticity equation.

The dominant overturning cell, analogous to North Atlantic Deep Water formation, is primarily controlled by the surface density contrast in the dominant hemisphere, which in turn is largely set by temperature. Consequently, in experiments with mixed boundary conditions, the dominant cell strength is relatively insensitive to the magnitude Q_S of the salinity forcing. However, Q_S strongly influences subordinate hemisphere properties, including the volume transport of a shallow overturning cell and the meridional extent of a tongue of low-salinity intermediate water reminiscent of Antarctic Intermediate Water.

The minimum Q_S is identified for which the steady, asymmetric flow is stable; below this value, a steady, equatorially symmetric, temperature-dominated overturning occurs. For high salt flux, the asymmetric circulation becomes oscillatory and eventually gives way to an unsteady, symmetric, salt-dominated overturning. For given boundary conditions, it is possible to have at least three different asymmetric states, with significantly different large-scale properties. An expression for the meridional salt transport allows one to roughly predict the surface salinity and density profile and stability of the asymmetric state as a function of Q_S and other external parameters.

1. Introduction

Though the earth's global thermohaline circulation is dominated by temperature (the deepest water is generally the coldest), salinity variations play a crucial role in determining the location of deep-water formation. The surface temperature distribution is roughly symmetric about the equator, but surface salinity has notable north–south asymmetries [e.g., cf. Figs. 8.8 and 8.10 in Peixoto and Oort (1992)], with winter northern North Atlantic water roughly 0.5 psu saltier than austral winter Weddell Sea water (Levitus and Boyer 1994). As a result, deep-water formation is equatorially asymmetrical within the World Ocean, with substantial transports of North Atlantic Deep Water crossing the equator and flowing into the Southern Hemisphere [Speer and McCartney (1991); Warren (1981) for a review of earlier work]. This asymmetry is interesting for purely oceanographic reasons as well as for its influence on climate. For example, the heat transport in the South Atlantic is equatorward rather than poleward (e.g., Macdonald 1993).

As Rooth (1982) and Bryan (1986) have shown, using a box model and a general circulation model, respectively, such an asymmetry in salinity and meridional overturning can occur even when the boundary conditions are equatorially symmetric. Surface boundary conditions form a relatively tight constraint on surface temperature but can be thought of as equivalent to specifying a flux of salinity rather than the salinity itself. Because of these ''mixed boundary conditions,'' more than one circulation state can exist given such a set of boundary conditions (Stommel 1961). In a single ocean basin spanning the equator, it is possible to have either equatorially symmetric temperature-dominated (*T*-dom) sinking near the poles, equatorially symmetric salinity-dominated (*S*-dom) sinking near the equator, or equatorially asymmetric deep-water formation at one pole only (Welander 1986).

Corresponding author address: Dr. Barry A. Klinger, Oceanographic Center, Nova Southeastern University, 8000 North Ocean Drive, Dania Beach, FL 33004.
E-mail: klinger@ocean.nova.edu

How overturning strength depends on external parameters has received relatively thorough scrutiny in single-basin systems driven by temperature-only boundary conditions (Bryan 1986; Colin de Verdiere 1988; Winton 1996; Marotzke 1997) or freshwater-only boundary conditions (Huang and Chou 1994). The two-hemisphere, mixed-boundary-condition case has been explored with two-dimensional models by Marotzke et al. (1988), Thual and McWilliams (1992), Quon and Ghil (1992, 1995), Cessi and Young (1992), Schmidt and Mysak (1996), Vellinga (1996), and Dijkstra and Molemaker (1997). When salinity forcing is sufficiently stronger than temperature forcing, only the *S*-dom state exists, and when temperature forcing is sufficiently stronger than salinity forcing, only the *T*-dom state exists. It is only when both temperature and salinity forcing are in some sense at intermediate strengths that the equatorially symmetric states and the asymmetric state can all exist [see Thual and McWilliams (1992) Fig. 3]. These two-dimensional studies did not relate the flow strength and regime boundaries to parameters that could be readily applied to three-dimensional basins in which basin width, planetary rotation, and planetary radius play a role. There has been no three-dimensional study of this system in which forcing parameters were systematically varied, though Weaver and Sarachik (1991) used such a model to study the time evolution of transitions from state to state.

The thermohaline circulation is a global system in which the flow in each basin is influenced by that in the other basins (Warren 1983; Gordon 1986; Rintoul 1991; Marotzke and Willebrand 1991; Stocker and Wright 1991; England 1993; Macdonald and Wunsch 1996). This system has an extremely complicated dependence on a multiplicity of parameters, including basin geometry (Hughes and Weaver 1994), atmospheric freshwater transports between basins (Marotzke and Willebrand 1991; Stocker et al. 1992), and the coupling to the atmosphere (e.g., Mikolajewicz and Maier-Reimer 1994; Rahmstorf and Willebrand 1995; Weber 1998). Therefore, it is useful to understand the less complicated, single-basin cell as a stepping stone to understanding the more complete system.

The basic question of this paper is: How do the external parameters in a two-hemisphere, mixed-boundary-condition system determine the temperature, salinity, and overturning in the equatorially asymmetric state? We subdivide this into two smaller problems. In the asymmetric state, one hemisphere will possess the densest surface water in the basin. Peterson (1979) and Cox (1989) have shown that this water must dominate the bottom of the entire basin (when the equation of state is linear), but the resulting state has not been carefully studied. Thus, given such an asymmetric surface density distribution, what is the resulting overturning strength and pycnocline structure? This will be examined in section 3, which discusses experiments in which the surface density is restored to a reference profile. Then the full question can be answered if, for a given mixed boundary condition, we can predict the resulting surface density. We consider this question via mixed-boundary-condition experiments in section 4.

Hughes and Weaver (1994) showed in an idealized global GCM under mixed boundary conditions that Atlantic overturning strength is linearly related to the basinwide meridional gradient in zonally and vertically averaged steric height (i.e., a double vertical integral of zonally averaged density). Rahmstorf (1996) found in his global GCM coupled to a diffusive atmospheric energy balance model that Atlantic overturning is proportional to the zonally averaged middepth density difference between northern and southern Atlantic boundaries. In contrast to these studies, we want to relate the strength of the thermohaline circulation directly to external parameters; to clarify the relation we use simpler geometry and forcing. Wang et al. (1999a,b) used an idealized, global, hybrid coupled GCM and Scott et al. (1999) uncoupled and coupled box models to study interhemispheric thermohaline flow and its interaction with the atmosphere, in particular the effects of equatorially asymmetric atmospheric water vapor transports. Here, we leave out asymmetries in forcing (except in restoring-boundary-condition experiments) and detailed considerations of ocean–atmosphere interactions, to focus on the rotating fluid dynamics of the interhemispheric thermohaline circulation. The impact of wind, nonlinearities in the equation of state, and north–south asymmetries in the forcing are all important factors that deserve careful treatment, and we defer these to a later paper. For simplicity we use a relatively idealized system here.

2. Numerical model

All experiments are conducted with MOM-2, the Modular Ocean Model version of the GFDL Model (Pacanowski 1996; Cox 1984), a B-grid (Arakawa and Lamb 1977) finite-difference discretization of the primitive equations that computes solutions by stepping forward in time. The domain is a sector of a sphere with zonal and meridional boundaries and a flat bottom. Default parameters are shown in Table 1; experiments with any of these parameters changed are noted in the text in section 4. The model is run at coarse, uniform horizontal resolution with vertical grid spacing increasing from 50 m at the surface to 500 m at the bottom. All advective terms are retained in the temperature, salinity and momentum equations, and density ρ is related to temperature T and salinity S by

$$\rho = \rho_0 + \beta S - \alpha T, \tag{1}$$

where α and β are the thermal and haline expansion coefficients, respectively. The values chosen correspond to a linearization of the equation of state at surface pressure and a temperature of about 13°C (see Table 1). Though Gargett and Holloway (1992) argue that dif-

TABLE 1. Summary of numerical experiments.

Parameter	Symbol	Value
Basin width, length	Λ, ϕ_p	60°, 64°
Basin depth	H	4500 m
Vert. diffusivity momentum, tracers	(ν_V, κ_V)	(1, 0.5) $\times$ 10^{-4} m^2 s^{-1}
Hor. diffusivity momentum, tracers	(ν_H, κ_H)	(250, 1.0) $\times$ 10^3 m^2 s^{-1}
Isopycnal diffusivity	κ_ρ	2000 m^2 s^{-1}
Expansion coefficients	α, β	0.2 kg m^{-3} C^{-1}, 0.8 kg m^{-3} psu^{-1}
T restoring timescale	τ	30 days
Long, lat grid spacing	$d\lambda$, $d\phi$	3.75°, 4.0°
Number of levels	N_z	15
Momentum time step	dt_M	3600 s
Tracer time step	dt_T	5 d

fusivities of T and S should be different, the parameterization of Zhang et al. (1998) shows this to be a relatively small effect; here we use the same diffusivity for both fields (see Table 1).

All walls and the bottom are insulating in both T and S. Temperature is forced by restoring the surface layer to a zonally uniform reference profile. The reference profile as a function of latitude ϕ in either hemisphere is given by

$$T = T_e + \frac{1}{2}\Delta T[\cos(\pi\phi/\phi_p) - 1], \qquad (2)$$

where $-\phi_p \le \phi \le \phi_p$, T_e is the restoring surface temperature at the equator, and ΔT is the restoring surface temperature difference between the equator and the polar boundary (in restoring boundary condition experiments, this is ΔT_N in the northern hemisphere and ΔT_S in the southern hemisphere). Thus as we move northward from the southern boundary, the restoring temperature smoothly increases from a low of $T_e - \Delta T_S$ to a high of T_e and then decreases back to a low of $T_e - \Delta T_N$.

In the restoring-boundary-condition runs (section 3), salinity is constant and hence no salinity forcing is necessary. In the mixed-boundary-condition runs (section 4), the reference temperature is symmetric about the equator ($\Delta T_N = \Delta T_S$). The salinity is driven by setting a zonally uniform surface salinity flux to represent the effects of freshwater fluxes produced by evaporation, precipitation, and runoff. The dependence on latitude for forcing strength Q_S is given by

$$q_S = Q_S \cos(\pi\phi/\phi_p)/\cos(\phi). \qquad (3)$$

This form represents the generally negative evaporation minus precipitation ($E - P$) at high latitudes and positive $E - P$ at low latitudes found on the real earth. The real earth also has a narrow region of negative $E - P$ near the equator, which we ignore here under the assumption that the resulting shallow equatorial salinity minimum has a relatively small effect on the large-scale thermohaline circulation. The cosine factor in the denominator is used so that the zonal integral of q_S would be a simple cosine in latitude, with no net salt added to or removed from the basin.

Experiments are started with initial conditions of either a resting, isothermal, isohaline (35 psu) ocean, or a previous experiment. Each run is integrated until a nearly steady state is reached, unless noted otherwise. The usual criteria for steady state being reached is that the drift in meridional volume transport exponentially decreases over the last several centuries of the integration and is no more than 0.0025 Sv per century (Sv $\equiv$ 10^6 m^3 s^{-1}) at the end. Spot checks on selected runs show that, when these criteria are met, other measures such as temperature and salinity are also nearly steady. In order to satisfy the Courant–Friedrichs–Levy criterion at the lowest computational cost, a shorter time step is used for the momentum equations than the tracer equations (Bryan 1984). Each experiment generally takes from 1000 to 5000 tracer years to reach steady state, which takes on the order of 1 day of cpu time on a DEC AlphaStation 250 4/266 workstation.

Most of the experiments are conducted using horizontal diffusion of properties to parameterize mixing induced by geostrophic eddies. Some runs with restoring boundary conditions are also repeated with the ''Gent–McWilliams'' parameterization, which supplements isopycnal diffusion of T and S with additional advection by a tracer velocity representing the untilting of isopycnals by baroclinic instability (Gent and McWilliams 1990; Gent et al. 1995). This parameterization has a stronger dynamical justification than horizontal diffusion, and allows numerical models to better represent the relatively thin thermocline and small deep-water formation regions of the real ocean and to eliminate spurious diapycnal diffusion in regions of strong horizontal gradients such as western boundary currents (Veronis 1975; Böning et al. 1995; Danabasoglu et al. 1994). The Gent–McWilliams runs are conducted with a flux-corrected transport scheme added to MOM-2 by Weaver and Eby (1997). Flux-corrected transport is a finite difference scheme that attempts to retain the accuracy of centered-difference schemes while also suppressing nonphysical overshoots of temperature and salinity (a property shared by the less accurate upstream differencing scheme).

3. Restoring boundary conditions

a. Experiments

We conduct two-hemisphere experiments, which are forced only by restoring to a temperature profile that is asymmetric about the equator. We wish to understand how the maximum meridional overturning volume transport and the pycnocline structure of a double-hemisphere overturning cell differ from the case of a single-hemisphere system. As section 4 will show, the surface density given by (2), with different values of ΔT in the

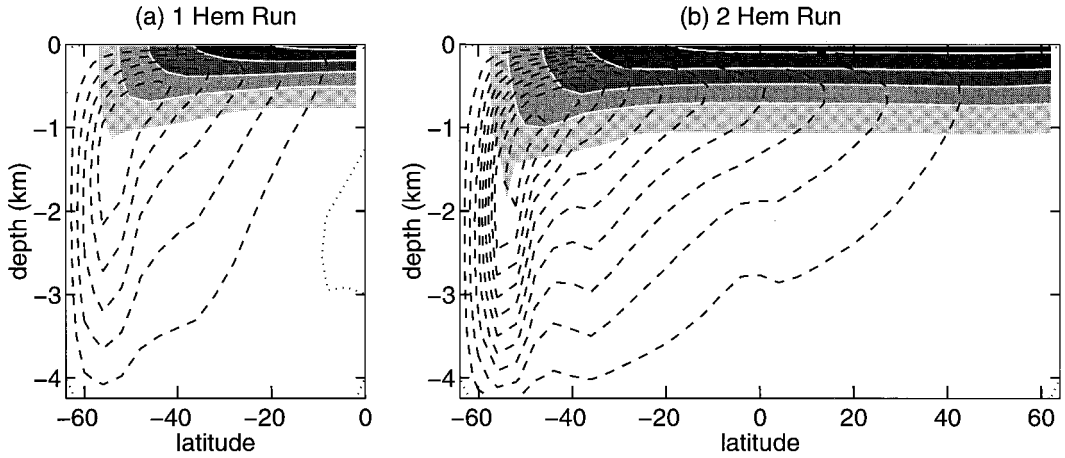

FIG. 1. Meridional overturning streamfunction (contours) and zonal average temperature (shading) for restoring BC experiments, (a) 1H and (b) 2H, $\Delta T_N = 0$. Overturning contours are 2 Sv apart; isotherms are at 0.05, 0.1, 0.2, 0.4, and 0.8 of $\Delta T_S = 30$°C. In this and all subsequent plots of overturning streamfunction, dashed, solid, and dotted contours represent negative (southern sinking), positive (northern sinking), and zero values, respectively.

northern and southern hemispheres, is a reasonable approximation to the shape of the surface density profiles produced by mixed-boundary-condition experiments.

In all the experiments, the southern hemisphere is made the ''dominant'' hemisphere by giving it the densest surface water. Thus the dominant deep water, analogous to North Atlantic Deep Water in the Atlantic Ocean, is formed in the southern hemisphere in our experiments. We chose the southern hemisphere because it happened to be the dominant hemisphere in the mixed-condition experiments (section 4); since our experiments have completely equatorially symmetric geometry (unlike the real ocean), the choice of dominant hemisphere is arbitrary. The weaker and deeper flow of Antarctic Bottom Water does not appear in these experiments because the equation of state is linear and there is no circumpolar channel corresponding to the Southern Ocean.

The relationship between the behavior in one-hemisphere (''1H'') and two-hemisphere (''2H'') basins is demonstrated by runs with ΔT_S set to 30°, 6°, and 1°C. In each of these experiments, we set $\Delta T_N = 0$, thus exploring the case of most extreme equatorial asymmetry first. For each 2H experiment, a 1H experiment is run with forcing identical to the dominant hemisphere of the corresponding 2H run. Outside of section 3b, ''1H experiment'' refers to an experiment with equatorial symmetry rather than an actual wall at the equator. These two variations are nearly identical (11.86 Sv overturning with the wall and 11.84 Sv with symmetry).

In another series of experiments, ΔT_S is fixed while ΔT_N is varied. We are especially interested in the situation in which ΔT_N is almost as large as ΔT_S. In this case, the degree of asymmetry between the hemispheres is small, yet the circulation must be qualitatively different from a symmetric experiment because deep water is required to spread from the dominant hemisphere to fill the deepest region of the other ''subordinate'' hemisphere. In this series of experiments, $\Delta T_S = 30$°C, while $\Delta T_P \equiv \Delta T_N - \Delta T_S$ is set to 15°, 6°, 3°, 1.5°, 0.6°, and 0°C.

b. Dependence on dominant hemisphere temperature gradient

The zonally integrated thermohaline circulation is characterized by small, relatively intense downwelling regions associated with deep convection and large areas of weak, diffusively driven upwelling (Fig. 1). In runs with $\Delta T_N = 0$, the presence of the nonconvecting hemisphere means that a strong thermocline covers about two times the area that it does in a single-hemisphere run.

The classical scaling for upwelling velocity W, thermocline depth D, and horizontal velocity V in large-scale, buoyancy-driven circulation (Bryan and Cox 1967; Bryan 1987; Colin de Verdiere 1988) is based on the vertical advective–diffusive balance,

$$wb_z = \kappa b_{zz}, \tag{4}$$

and thermal wind,

$$fv_z = -b_x, \tag{5}$$

where f is the Coriolis parameter, v and w are meridional and vertical velocities, and $b = -g\rho/\rho_0$ is the buoyancy (g is the gravitational acceleration, 9.8 m^2 s^{-1}). These equations yield the scale relations

$$W = \kappa/D, \tag{6a}$$

$$fV/D = \Delta b/M, \tag{6b}$$

where Δb is the imposed meridional surface buoyancy range and M is the basin zonal length scale. One might ask whether the zonal buoyancy difference in (5) must

scale like Δb, but Marotzke (1997) demonstrates that this is actually a reasonable assumption, and we show below that it holds fairly well in our numerical experiments. Another weakness of the classical scaling employed here (and indeed of the vertical mixing parameterization in the model) is that vertical or diapycnal mixing in the ocean is known not to be uniform but concentrated near the margins (e.g., Munk 1966; Wunsch 1970; Armi 1978; Ledwell and Bratkovich 1995; Toole et al. 1997). Again, Marotzke (1997) has shown that some scaling and numerical results are reasonably insensitive to assumptions about how localized the mixing is.

One more scale relation must be included in order to close the system and find W, D, and V. Often this is done using the linear vorticity relation (see Bryan 1987; Colin de Verdiere 1988),

$$\beta_0 v = f w_z, \tag{7}$$

where β_0 is the meridional gradient of f. However, this equation does not apply to the western boundary current, an important contributor to the zonal average of v. When κ or Δb is varied, this inapplicability does not matter, because the western boundary current strength has the same sensitivity to κ and Δb as the interior flow. However, the relationship between the western boundary and the interior currents changes when the geometry of the flow changes. Thinking of the deep flow as a homogeneous layer driven by a point source and a distributed sink (Stommel et al. 1958; Stommel and Arons 1960), we see that, if the sink area is changed but upwelling speed w remains the same, the interior flow is unaffected but the western boundary current must change to satisfy continuity. In order to compare 2H flows to 1H, it is therefore more appropriate to use the continuity equation (see Marotzke 1997; Winton 1996).

Assuming that the volume transport into the region of deep-water formation equals the upwelling over almost the entire basin, we have

$$MDV = MLW, \tag{8}$$

where L is the meridional length of the basin. Equations (6) and (8) yield the scale relations

$$D = \left(\frac{\kappa L M f}{\Delta b}\right)^{1/3}, \tag{9a}$$

$$W = \left(\frac{\Delta b \kappa^2}{f L M}\right)^{1/3}, \tag{9b}$$

$$V = \left(\frac{\Delta b^2 \kappa L}{M^2 f^2}\right)^{1/3}, \tag{9c}$$

$$\Phi = MDV = \left(\frac{\Delta b \kappa^2 L^2 M^2}{f}\right)^{1/3}, \tag{9d}$$

where Φ is the meridional overturning streamfunction. If linear vorticity (7) were used instead of continuity (8), then (9) would be the same except that L would be replaced with the radius of the earth, R. In one hemisphere, $L \approx R$, and the two assumptions about the vertical velocity scale would yield the same result. In two hemispheres with one of them nonconvecting, however, $L \approx 2R$, and thus the scaling containing the continuity equation predicts that the two-hemisphere case will have a broader thermocline and weaker vertical velocity, whereas scaling containing the linear vorticity equation predicts that the thermocline and vertical velocity will be the same in the two cases.

We test the above scaling relationships with 2H ($\Delta T_N = 0$) and 1H experiments. In the 1H experiments, $D \propto \Delta b^{-1/3}$ and $w \propto \Delta b^{1/3}$, as expected. Here, D is taken to be the integral length scale of the zonal average temperature at the equator,

$$D = \left(\int_{z_0}^{0} zT\, dz\right) \Big/ \left(\int_{z_0}^{0} T\, dz\right). \tag{10}$$

In each run, water with temperature in the bottom 1% of the temperature range for the water column is considered ''subthermocline'' and is excluded from the calculation. Here W is found by taking the maximum zonal average vertical velocity at each latitude and averaging this from latitudes 2° to 30°S, which is much of the region dominated by upwelling but excludes recirculation close to the convection region. The total volume transport of the meridional overturning cell is also roughly proportional to $\Delta b^{1/3}$, though this scaling law is closer to $\Delta b^{1/2}$ for small Δb because the upwelling area decreases somewhat for smaller Δb.

The maximum buoyancy difference between the eastern and western boundaries is approximately $b_E - b_W = 0.25\Delta b$ for all 1H and 2H runs, confirming the theoretical result of Marotzke (1997) and the hypothesis that the zonal buoyancy difference scales like Δb. The zonal buoyancy difference has a weak dependence on L (2H runs have about a 20% smaller proportionality constant). All these minor factors can be ignored in (9).

The factors of $L^{1/3}$ in (9) imply that, since $2^{1/3} = 1.3$, each 2H run should have a 30% broader thermocline and 30% weaker upwelling than the corresponding 1H run. We measure the thermocline depth at the equator as before, and average the maximum zonal average w from 30°S to 62°N. The numerical experiments display the relationship between 2H and 1H D and W predicted by the scaling.

The combination of a somewhat weaker W and a larger area of upwelling cause the total overturning volume transport of the 2H experiments to be somewhat less than double that of the 1H experiments: the scaling predicts a factor of $2^{2/3} = 1.6$, whereas actual values are slightly higher (Table 2). Roughly equal amounts of upwelling occur in both hemispheres. For ΔT_S of 30°C and 6°C, the convecting hemisphere has somewhat greater upwelling than the nonconvecting hemisphere. The western boundary current is stronger in this hemi-

TABLE 2. Restoring runs, one and two hemisphere (hem) overturning. All transports given in Sv. For 2-hem runs, $\Delta T_N = 0$.

ΔT_S	1-hem	2-hem	Cross-eq.	2-hem/ 1-hem	Cross/ 2-hem
30	11.9	21.2	8.2	1.8	0.39
6	6.9	13.3	5.1	1.9	0.38
1	2.5	5.0	2.8	2.0	0.56

sphere (see Fig. 1) so that horizontal mixing there brings additional diapycnal mixing and enhances upwelling (Veronis 1975; Böning et al. 1995). In the $\Delta T_S = 1$°C run, the smaller upwelling area in the convecting hemisphere makes this hemisphere's fraction of total upwelling smaller. Ignoring these details, however, the striking feature of these experiments is the simplicity of the relationship between flow magnitudes in the 2H and 1H cases. As the experiments show, the same relationship between 2H and 1H cases persist for ΔT_S varied by a factor of 30 and corresponding thermocline depths ranging from a narrow surface region to nearly the entire water column.

Hughes and Weaver (1994) found a linear relationship between overturning strength Φ and the pole-to-pole difference in vertically integrated steric height, Ψ. We show now that this is consistent with the scaling (9) above. Since Ψ is the double vertical integral of meridional buoyancy difference, $\Psi \propto \Delta b D^2$. Substituting (9a) for D, we have

$$\Psi \propto (\Delta b \kappa^2)^{1/3}, \tag{11}$$

and combining this with (9d), we predict that Ψ should indeed be proportional to Φ.

c. Dependence on subordinate hemisphere temperature gradient

For $0 < \Delta T_P < \Delta T_S$, the southern-sinking cell still dominates the circulation, but a weaker subordinate cell now forms in the near-surface water of the northern basin (Fig. 2). We assume that the $\Delta T_P = \Delta T_S$ case can provide a crude estimate of how deep the northern cell extends. The minimum temperature of water sinking in the northern hemisphere is ΔT_P (actually a little less, due to the restoring boundary condition). Thus, for $\Delta T_P = 3$°C, for example, the northern sinking should not penetrate the 3°C isotherm. Since the vertical temperature gradients are small below the top kilometer, the southern cell will dominate almost the entire northern hemisphere water column unless ΔT_P is nearly zero. However, as Fig. 2 and Table 3 show, the maximum depth of the northern overturning cell actually reaches much deeper than either the ΔT_P isotherm or the northern mixed layer. In sum, the penetration depth of the subordinate cell is clearly related to the mixed layer depth but, since the meridional overturning is proportional to a double vertical integral of the density difference between eastern and western walls, one cannot expect a simple correspondence [see Marotzke (1997) for a detailed discussion].

The abrupt change between the symmetrical forcing and asymmetrical forcing is perhaps most strongly reflected in the cross-equatorial transport (Fig. 3a), which is zero for the symmetric forcing and about 7 Sv for all other runs with $\Delta T_S = 30$°C (for comparison, the 1H overturning is 11.8 Sv). The strength of the southern sinking region also jumps, going from about 12 Sv to about 20 Sv as ΔT_P increases from 0, and the northern sinking overturning decreases abruptly. These values are given approximately by

$$\Phi_{\pm} = \Phi_0[1 \pm (\Delta T_P/\Delta T_S)^{1/6}], \tag{12}$$

where Φ_0 is the volume transport for the 1H experiment, and Φ_+, Φ_- are the volume transports of the strong, deep (''dominant'') southern cell and the weak, shallow (''subordinate'') northern cell, respectively. The origin of the exponent is not clear. The sum of the volume transports of the two cells is nearly independent of ΔT_P, perhaps because the total upwelling is a function of the overall thermocline structure, which is not strongly sensitive to ΔT_P. As ΔT_P is decreased, the tropical and midlatitude thermocline gets narrower (see previous subsection), thus promoting stronger upwelling, but the northern thermocline is eroded, thus decreasing the area of upwelling.

Asymmetrical overturning carries heat across the equator from the subordinate hemisphere to the dominant hemisphere. Although the cross-equatorial volume transport is not strongly dependent on the degree of asymmetry between northern and southern hemisphere surface density, the cross-equatorial heat transport is roughly proportional to $\sqrt{\Delta b_P/\Delta b_S}$ (Fig. 4), where again the subscripts P and S stand for pole-to-pole and southern hemisphere differences, respectively. We plot heat transport as a function of Δb rather than ΔT in order to facilitate comparison with mixed-boundary-condition runs in the next section. As Δb_P goes to zero, the top of the dominant cell gets pushed down below the thermocline in the subordinate hemisphere. Thus, at the equator, the shallower limb of the dominant cell approaches the temperature of the deeper limb (Fig. 2). Overturning streamlines are not pushed down as far in the southern hemisphere so that the maximum southward heat transport (which occurs in the southern hemisphere) is only somewhat more sensitive to $\Delta b_P/\Delta b_S$ than the dominant cell volume transport. In the northern hemisphere, heat transport is all directed southward for sufficiently weak subordinate cell strength ($\Delta b_P/\Delta b_S \geq 0.5$). For smaller Δb_P, the peak northward heat transport is roughly proportional to the subordinate cell volume transport.

d. Gent–McWilliams runs

The experiments with $\Delta T_S = 30$°C and $\Delta T_P = 0$°, 0.6°, 3°, and 30°C are repeated with the Gent–Mc-

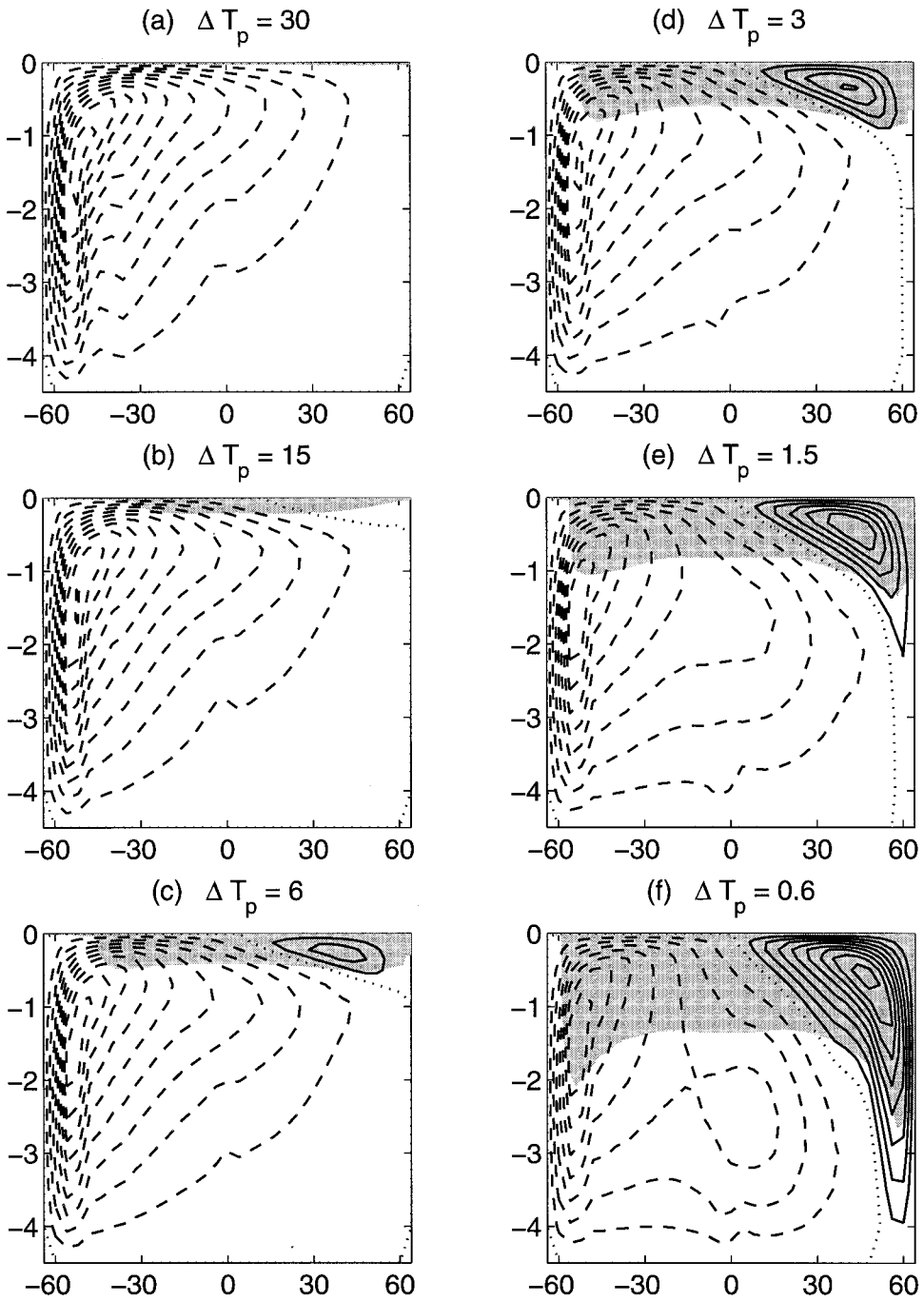

FIG. 2. Meridional overturning streamfunctions for runs with $\Delta T_S = 30$°C and various $\Delta T_N < \Delta T_S$. Contour intervals are 2 Sv for dashed contours and 1 Sv for solid. Shading represents the temperature range ventilated in both hemispheres (all water warmer than subordinate hemisphere minimum sea surface temperature).

Williams parameterization. These runs display the known features of isopycnal mixing: thinner thermocline and upper limb of overturning circulation, more compact downwelling region, and reduction of midlatitude upwelling. However, the key features described in the subsections above remain in these runs. The experiment with $\Delta T_P = \Delta T_S$ has a broader thermocline and weaker w than the $\Delta T_P = 0$ run (because of the imposed symmetry, the latter is essentially a 1H run). In runs with a subordinate cell, the cell reaches deeper than would be predicted by looking at the northern mixed layer or the $\Delta T_P = 0$ stratification. Thus neither of these features can be attributed to the deficiencies of horizontal mixing. The volume transports in each cell and

TABLE 3. Subordinate overturning cell depth. D_{cell} is the maximum depth of the subordinate cell, $D_{\Delta T_P}$ is the depth of the ΔT_P isotherm in the $\Delta T_P = \Delta T_S$ run, and D_{mixed} is the mixed layer depth. All depths are in m.

ΔT_P	D_{cell}	$D_{\Delta T_P}$	D_{mixed}
15	400	240	0
6	800	500	425
3	1600	720	825
1.5	bottom	1050	1600

across the equator are somewhat less sensitive to ΔT_P for weak asymmetries and more sensitive for strong asymmetries, compared to the horizontal mixing runs [equivalent to a larger exponent in (12)], but the magnitudes are still quite similar (Fig. 3). Why we find an apparently much reduced sensitivity to the eddy stirring parameterization than Weaver and Eby (1997) is not clear. Their Gent–McWilliams experiment had an overturning strength consistent with our 1H Gent–McWilliams run, but their horizontal-mixing experiment had much stronger overturning than ours.

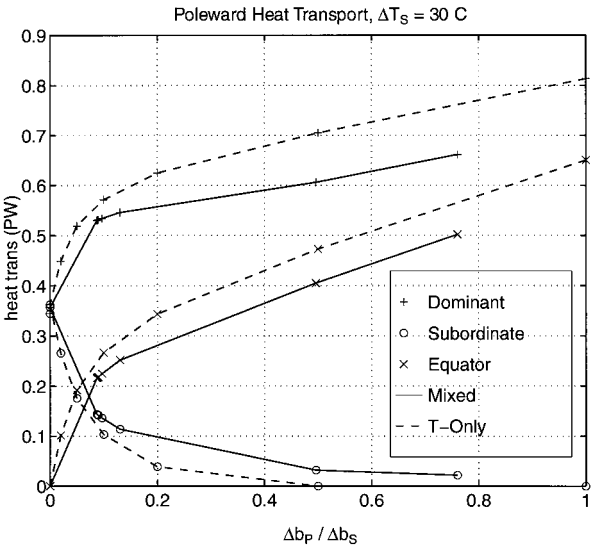

FIG. 4. Meridional heat transport as a function of $\Delta b_P/\Delta b_S$ for temperature-only (dashed) and mixed-boundary-condition (solid) experiments, including values at the equator (×), the southward (dominant) maximum (+), and the northward (subordinate) maximum (○).

4. Mixed boundary conditions

a. Temperature-dominated, salinity-dominated, and asymmetric states

The previous section took the surface density distribution as an almost prescribed external parameter. In reality, however, it is a function of salinity whose distribution is influenced by the ocean circulation more strongly than is temperature. Hence, we now turn to a model driven by mixed boundary conditions, where we still restore surface temperature as before but apply a fixed surface freshwater flux. Apart from showing the model's response to large variations in the latter, we

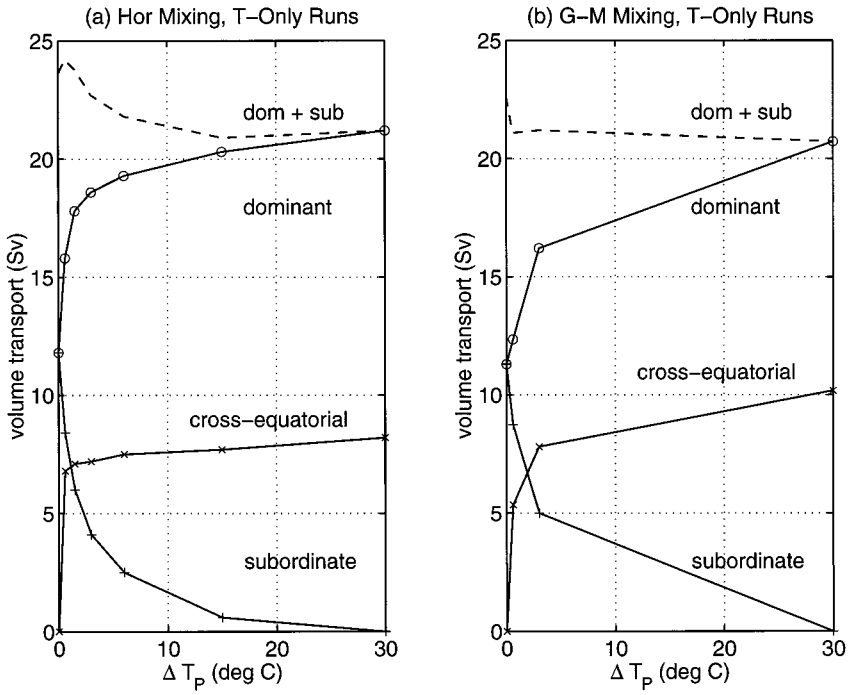

FIG. 3. Volume transport as a function of ΔT_P for the dominant cell, subordinate cell, sum of dominant and subordinate cells, and cross-equatorial flow. (a) Experiments with horizontal diffusion. (b) Experiments with Gent–McWilliams mixing (advective plus eddy components).

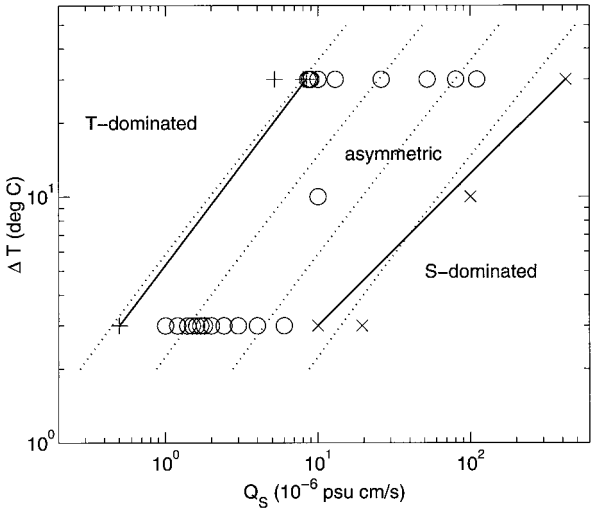

FIG. 5. Salt flux Q_S and imposed temperature difference ΔT for mixed-boundary-condition experiments with $\kappa_H = 1000$ m^2 s^{-1}. Locations in parameter space are denoted by a "+" if only *T*-dom states were found, by a "×" if only *S*-dom states were found, and by an "○" if at least one asymmetric state was found. Solid lines represent estimates of regime boundaries. Dotted lines are estimates of $Q_S(\Delta T)$ for constant *s* values of 0.1, $\sqrt{0.1}$, 1, and $\sqrt{10}$ (section 4b). Here, s is the nondimensional subordinate hemisphere salinity gradient, normalized by its influence on density relative to ΔT.

will, through scaling arguments, link the strength of the salt forcing to pole-to-equator and pole-to-pole salinity and density difference, at which point the results from the previous section apply.

We now consider the two-hemisphere system with surface temperature restored to the reference profile given by (2) and with surface salt flux given by (3). According to the work of Thual and McWilliams (1992) and others, one would expect that given the imposed temperature difference ΔT, if the salt flux Q_S is sufficiently small, the only possible circulation is a symmetric *T*-dom overturning. Similarly, for sufficiently high Q_S, the only solution should be a symmetric *S*-dom overturning. It is only at intermediate values of Q_S that the asymmetric mixed state occurs. Numerical experiments are conducted for $\Delta T = 30$°C and 3°C using many values of Q_S and for $\Delta T = 10$°C using a few values of Q_S. The unrealistically small temperature differences (3°C and 10°C) are used in order to better understand how circulation depends on ΔT. To isolate the importance of the diffusion term in the salt transport equation below, additional $\Delta T = 30$°C experiments are performed with κ_H five times the default value. Large κ_H is not realistic for the ocean, but salt transport box models can use horizontal diffusion to mimic the effect of wind-driven gyres (Thual and McWilliams 1992), which is crucial for the stability of the thermohaline circulation under mixed boundary conditions (Marotzke 1990). Hence, it is interesting to establish diffusive behavior for comparison with future wind-driven experiments. Other $\Delta T = 30$°C experiments are conducted with weaker restoring to the reference temperature (a timescale of $\tau = 300$ d rather than the default 30 d timescale). This complicates the relationship between surface density and surface salinity, but may be more realistic for the large spatial scales considered here (e.g., Rahmstorf and Willebrand 1995; Marotzke and Pierce 1997).

TABLE 4. Series of mixed BC experiments, asymmetric state. External parameters and some solution characteristics of the mixed-boundary-condition runs. Min and max refer to minimum and maximum values for which an asymmetric state was found (not including slightly asymmetric states in $\Delta T = 3°$ runs). Here, ΔT is in °C, κ_H is in m^2 s^{-1}, τ is in days, and Q_S is in 10^{-6} psu cm s^{-1}

ΔT	Comments	min Q_S	max Q_S	min *s*	max *s*
30		8.4–8.6	110–420	0.15	1.3
3		<1	6–10	0.35	1.5
30	$\kappa_H = 5000$	28–30	150–200	0.31	1.6
30	$\tau = 300$	17.6–17.8	100–110	0.33	1.3

Figure 5 shows a broad brush picture of where in the (ΔT, Q_S) parameter space asymmetric states exist (see also Table 4). For comparison, typical large-scale surface freshwater flux in the ocean is around 50 cm yr^{-1} (Schmitt et al. 1989; Wijffels et al. 1992). For a surface salinity of 35 psu, a freshwater flux of 1 cm yr^{-1} is equivalent to salt flux of about 10^{-6} psu cm s^{-1}. For convenient comparisons, all Q_S values will be stated in units of 10^{-6} psu cm s^{-1} unless noted otherwise.

For most of the runs, the solution eventually approaches steady state based on the criteria described in section 2. These states generally have overturning cells and pycnocline structures qualitatively similar to the restoring boundary condition experiments of section 3. Typical surface salinity has a broad equatorial maximum, a weak southern polar minimum, and a strong northern polar minimum (Fig. 6a). Southern polar salinities are nearly identical between the experiments because most of the model volume is filled with this water. This means that southern polar salinity is near the globally averaged salinity, which is the same for all experiments. The freshness of the northern surface water makes the surface density profile asymmetric (Fig. 6b), as assumed in section 3. The surface density range in the dominant hemisphere is only modestly affected by the strength of the salinity forcing, whereas Q_S is a dominant influence on the density range in subordinate hemisphere. The surface temperature range is greater in the subordinate hemisphere than in the dominant hemisphere because the residence time of high-latitude surface water is somewhat longer in the subordinate hemisphere, giving the water more time to cool to the restoring temperature. In experiments with strong surface restoring, the surface temperature range in the two hemispheres is the same to within a few percent. However, in the weak restoring experiments, the temperature range is about 20% less in the dominant hemisphere, where the coldest surface water is around 5°C.

For large Q_S, no steady states are found. One such

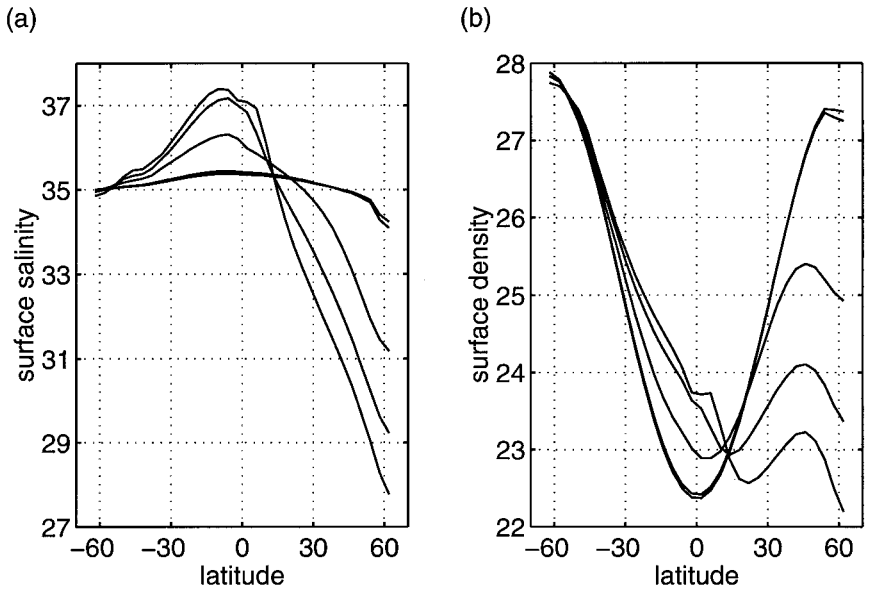

FIG. 6. Zonal average surface (a) salinity and (b) density for several $\Delta T = 30$ experiments ($Q_S = 8.6, 10, 26, 52, 80$). Salinity range and temperature asymmetry both increase with Q_S.

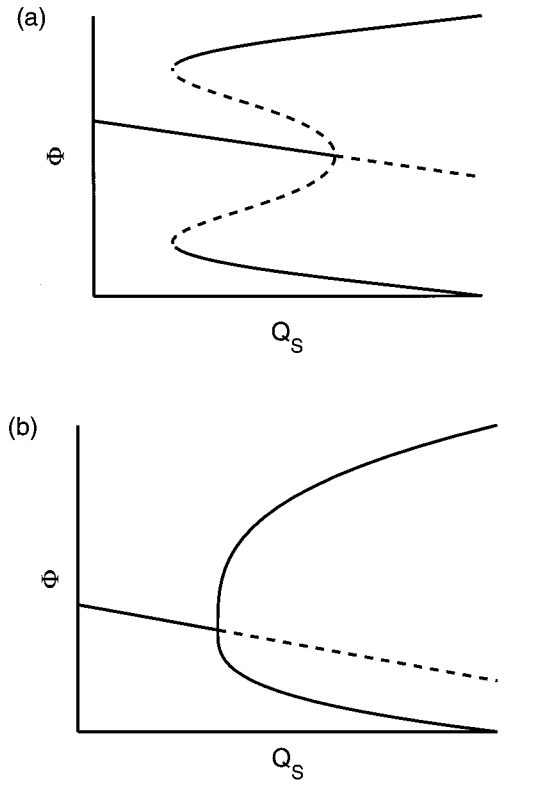

FIG. 7. Schematic of overturning transport maximum vs Q_S showing (a) subcritical and (b) supercritical pitchfork bifurcation (Drazin 1992). Solid lines are stable equilibria, while dashed lines are unstable equilibria. Upper curve is Φ_+, lower curve is Φ_-, and central curve is symmetric state.

run (default κ_H, $\Delta T = 30$°C, $Q_S = 110$) has an asymmetric overturning in which the dominant cell oscillates from a relatively weak, shallow overturning to a deeper, stronger overturning; the period is roughly 300 yr. A counterrotating high-latitude cell also appears at irregular periods. In the *S*-dom runs, the meridional overturning is usually confined to the top kilometer or so of the water column, with ''flushes'' of strong, deep equatorially asymmetric overturning occuring now and then. The shift from steady to oscillating states as salinity forcing is increased has also been seen in single-hemisphere systems (Weaver et al. 1991, 1993; Winton and Sarachik 1993; Huang 1994); thermohaline oscillations in two-hemisphere basins have been reported by Weaver and Sarachik (1991).

Dijkstra and Molemaker (1997) showed that for a two-dimensional model, the temperature restoring timescale and the exact form of $q_S(\phi)$ can change qualitative aspects of the equilibrium curves of $\Phi_+(Q_S)$. If $q_S(\phi)$ has maxima at the polar boundaries [as in our experiments and in Thual and McWilliams (1992)] the system can have a subcritical pitchfork bifurcation, which allows stable equilibria to coexist in some range of Q_S [Fig. 7a; see also Dijkstra and Molemaker (1997) Figs. 15 and 16]. However, if the $q_S(\phi)$ maxima are equatorward of the polar boundaries (as in Marotzke et al. 1988; Vellinga 1996), the system has a supercritical pitchfork bifurcation, in which the symmetric state is unstable when the asymmetric state is stable [Fig. 7b; also Dijkstra and Molemaker (1997, Fig. 4)].

We explored the multiple equilibria of the system by varying the initial condition for given parameters (Fig. 8). The behavior of the asymmetric state in our experiments is consistent with a subcritical bifurcation. All

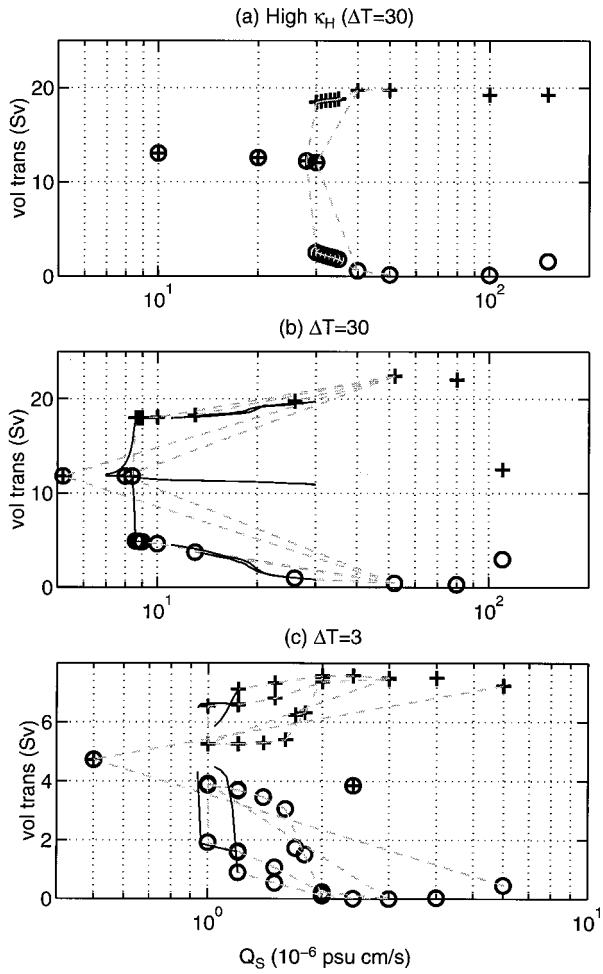

FIG. 8. Total volume transport of the dominant (''+'') and subordinate (''○'') meridional overturning cells as a function of Q_S (in units of 10^{-6} psu cm s^{-1}, which roughly corresponds to cm yr^{-1} of surface freshwater flux) for (a) $\kappa_H = 5000$ m^2 s^{-1}, (b) $\Delta T = 30$°C, and (c) $\Delta T = 3$°C experiments. Each dashed line connects an experiment to the experiment that is used as an initial condition (initial condition runs were generally at higher Q_S than succeeding runs). Solid lines show values for runs in which Q_S is changed continuously during the run. The *S*-dom experiments are not shown. In (b), the highest Q_S experiment data is based on a time-average of the oscillating series.

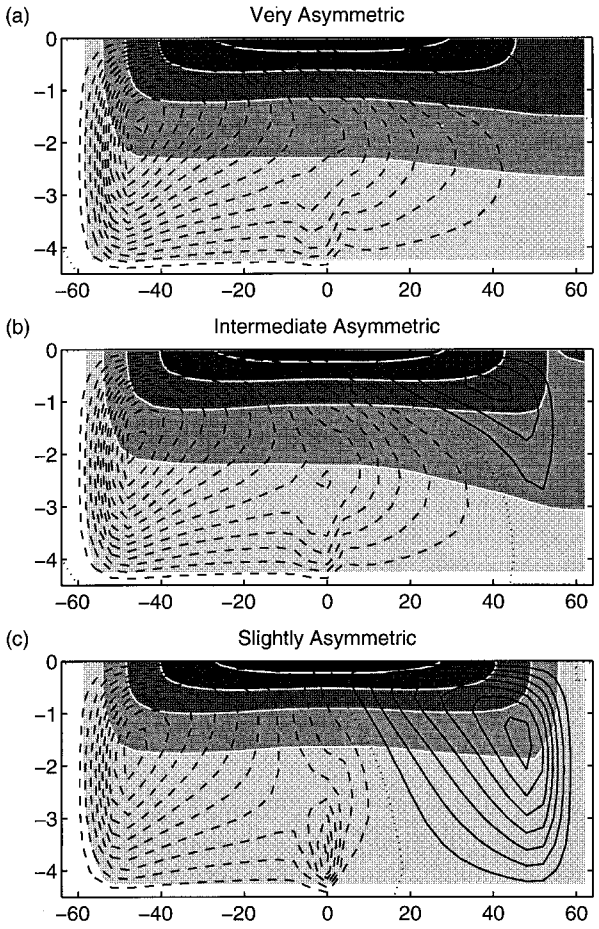

FIG. 9. Meridional streamfunction and zonal average density for (a) very asymmetric, (b) intermediate asymmetric, and (c) slightly asymmetric states with $\Delta T = 3$°C and $Q_S = 1.2$. Streamfunction contour interval is 0.5 Sv; isopycnals are at (28 kg/m^3 − ρ), where ρ is 0.025, 0.05, 0.1, 0.2, and 0.4 kg m^{-3}.

three series of experiments shown in Fig. 8 have both symmetric ($\Phi_+ = \Phi_-$) and asymmetric ($\Phi_+ \neq \Phi_-$) circulations for overlapping ranges of Q_S. In a supercritical bifurcation, as Q_S is lowered, the dominant and subordinate transports converge until they become equal at a critical Q_S. In our experiments, no such transition region is evident; a small decrease in Q_S pushes a strongly asymmetric system into a *T*-dom state (see, e.g., Fig. 8b, $8 < Q_S < 9$). In several experiments, we vary Q_S continuously over the course of a few thousand years. For the $\Delta T = 30$°C, default κ_H series, these confirm the abrupt transition to the *T*-dom state and shows that the *T*-dom state is stable for $Q_S < 26$, above which the equatorial asymmetry begins to grow. We further test the stability of the *T*-dom state by imposing a pole-to-pole surface salinity difference of 0.2 psu for ten years on one high-Q_S symmetric state ($\Delta T = 30$, default κ_H, $Q_S = 10$). This produces a small asymmetry in the overturning, which virtually disappears within 1000 yr.

The series of experiments with $\Delta T = 30$°C (Figs. 8a,b) exhibit the states displayed in two-dimensional experiments: a *T*-dom, *S*-dom (not shown), and asymmetric state. The $\Delta T = 3$°C case is more complicated (Fig. 8c). For overlapping ranges of Q_S, there are at least *three* asymmetric states, a ''very'' asymmetric state in which the dominant state cell is much stronger than the subordinate cell (Fig. 9a), an ''intermediate'' asymmetric state (Fig. 9b), and a ''slightly'' asymmetric state in which the dominant and subordinate cells are nearly equal in strength (Fig. 9c).

The streamfunction disturbance in the equatorial deep ocean in Fig. 9c may be due to the numerical instability identified by Weaver and Sarachik (1990). We attempted

to eliminate this disturbance both by increasing the vertical viscosity from 1 $cm^2\ s^{-1}$ to 10 $cm^2\ s^{-1}$ and by roughly doubling the vertical resolution. Neither method worked; however, the higher resolution runs helped us discover the intermediate asymmetric state, which we were then able to maintain with the default vertical resolution.

Which state a given experiment falls into depends on the initial condition for the experiment. Starting at the very asymmetric state with $Q_S = 3$, when Q_S is decreased in small increments, the solution remains in a very asymmetric state for $Q_S \geq 1.2$. Starting with the same $Q_S = 3$ initial condition, but immediately lowering Q_S to 1, the system moves into the slightly asymmetric state, which it maintains as Q_S is increased to 1.6. When the slightly asymmetric run with $Q_S = 1$ is used as an initial condition for a high vertical resolution run with the same Q_S, the system falls into the intermediate asymmetric state. This state persists when Q_S is raised to 1.2 and when this $Q_S = 1.2$ run is continued at the default (low) vertical resolution. These pathways between various states indicate that relatively small perturbations in the initial state can change the final state of the system. It is not clear how many more asymmetric states exist in this parameter range. Various $\Delta T = 30$°C experiments with different initial conditions do not reveal any multiple asymmetric states.

b. Properties of asymmetric states

1) SALT TRANSPORT AND SURFACE SALINITY RANGE

The meridional salt transport is imposed by the surface salt flux Q_S, but the manner in which this constraint is satisfied is determined by the flow field. Given some knowledge about the behavior of the flow field, we can predict the meridional surface salinity gradient in the subordinate hemisphere as a function of Q_S.

We start by the standard decomposition of meridional transports into the overturning component (proportional to the vertical correlation of zonally averaged velocity and property), gyre component (correlations between the deviations from the zonal means of velocity and property), and diffusive components. In our numerical experiments with an asymmetric circulation, the gyre component is small in the midlatitude subordinate hemisphere (figure not shown). Therefore we neglect the gyre component and obtain an approximate balance between the surface flux [Eq. (3)] integrated over half the hemisphere and the midlatitude meridional transport:

$$[a\Phi/4 + (M/L)\kappa_H \Delta z]\Delta S = LMQ_S/\pi, \qquad (13)$$

where Φ is the overturning volume transport, ΔS is the surface salinity range in the subordinate hemisphere, Δz is the depth of the halocline, L and M are the meridional and zonal (at the equator) lengths of a hemisphere, and a is the fraction of total overturning that occurs in the polar half of the nonconvecting basin. The Φ term is divided by a factor of 2 because S varies smoothly with depth, and by another factor of 2 because the salinity difference between the midlatitude surface and the deep water is approximately $\Delta S/2$.

The volume transport Φ is not an external parameter. According to the experiments of the previous section, it should be about twice the size of the overturning in a symmetric $Q_S = 0$ system. This overturning can be related to external parameters by Eq. (9d). We assume that about one-quarter of the upwelling occurs in the northern quarter of the basin, so $a = ¼$. We also assume that Δz is approximately the pycnocline depth [obtainable from Eq. (9a)].

A useful parameter to consider is the dimensionless salinity gradient $s = \beta\Delta S/\alpha\Delta T$, the relative contribution to density of salinity and temperature. Regardless of the actual values of ΔT and ΔS, two systems with the same s should have about the same degree of density asymmetry and the same relative strengths of dominant and subordinate cells. For a given s, the relationship between ΔT and Q_S can be made clear by combining (13) with the scaling laws discussed in section 3. From (9), we have $\Phi = \Phi_r(\Delta T/\Delta T_r)^{1/3}$ and $\Delta z = \Delta z_r(\Delta T/\Delta T_r)^{-1/3}$, where Φ_r and Δz_r are reference values for Φ and Δz at some reference temperature range ΔT_r. Then (13) can be written

$$Q_S = Q_0\left[1 + k\left(\frac{\Delta T}{\Delta T_r}\right)^{-2/3}\right]\left(\frac{\Delta T}{\Delta T_r}\right)^{4/3} s, \qquad (14)$$

where the relative strength of the diffusivity term is represented by

$$k = \frac{(M/L)\kappa_H \Delta z_r}{a\Phi_r/4} \qquad (15)$$

and the normalization for Q_S is given by

$$Q_0 = (\pi/4)a\Phi_r \Delta T_r(\alpha/\beta)/LM. \qquad (16)$$

As Fig. 10 shows, (14) gives a roughly correct characterization of s versus Q_S/Q_0, with predicted values of s about ⅔ of actual values. Therefore, most of the variation in ΔS, which spans nearly two orders of magnitude in the experiments, can be explained by (14). The estimates in Fig. 10 use $\Delta T_r = 30$°C, for which we use the default κ_H, symmetric state to give us $\Phi_r = 23.6$ Sv (total overturning) and $\Delta z_r = 190$ m (integral depth scale of equatorial pycnocline). The diffusive term $k(\Delta T/\Delta T_r)^{2/3}$ is only 0.12 for $\Delta T = 30$°C (default κ_H) but is about 0.6 for high κ_H and for $\Delta T = 3$°C.

The actual ranges of s for the asymmetric state are shown in Table 4. Whereas asymmetric states exist for quite different ranges in Q_S for $\Delta T = 3$°C and $\Delta T = 30$°C, the ranges in s are quite similar. Similarly, curves of $Q_S(\Delta T)$ for s constant are nearly parallel to the regime boundaries of the asymmetric state (see Fig. 5). It is also interesting that the two series of experiments with

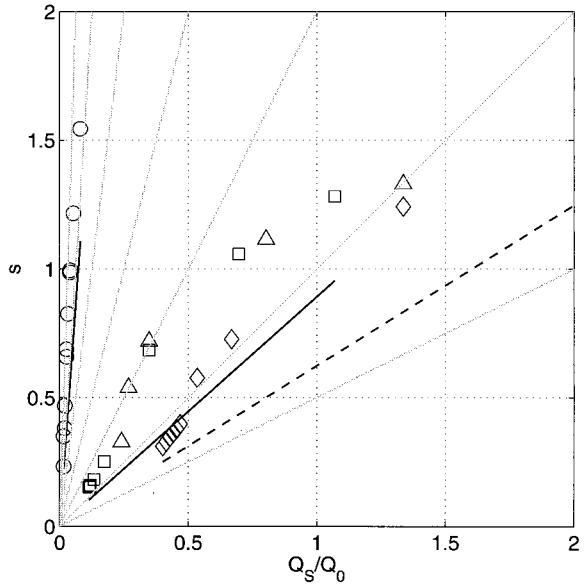

FIG. 10. Dimensionless salinity gradient s as a function of dimensionless salinity flux Q_S/Q_0 for asymmetric-state runs. $\Delta T = 3$ runs are represented by circles; $\Delta T = 30$ runs are represented by squares (default κ_H), diamonds (high κ_H), and triangles (weak temperature restoring). Black lines are estimates based on (14), with dashed line for high κ_H runs. For reference, gray lines mark slopes of 0.5, 1, 2, 4, 8, and 16.

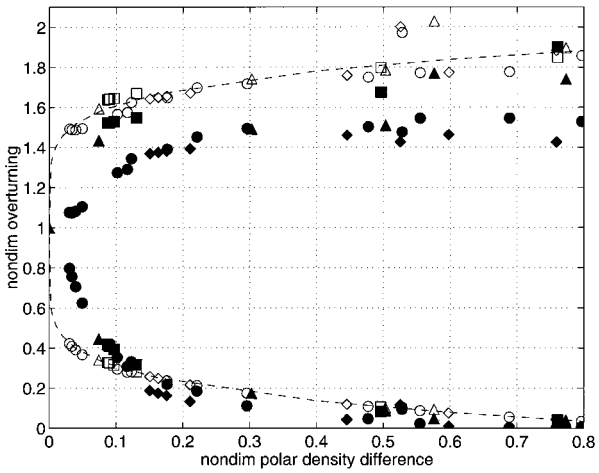

FIG. 11. Total volume transport of dominant and subordinate cells as a function of polar buoyancy difference Δb_P for $\Delta T = 3$°C (circles) and $\Delta T = 30$°C (squares for default κ_H, diamonds for high κ_H, and triangles for weak restoring). Volume transport and buoyancy difference in each series of experiments are normalized by values from corresponding $Q_S = 0$ (T-dom state) experiments. Filled symbols represent experiments, open symbols represent prediction based on Δb_P and Δb_S (i.e., changes in dominant hemisphere buoyancy differences are taken into account), and dashed lines represent predictions based on Δb_P alone (dominant hemisphere buoyancy differences are assumed constant).

a strong diffusive term in (14) have nearly identical ranges of s.

2) SURFACE DENSITY AND OVERTURNING STRENGTH

We now link the salinity to the buoyancy and from there to the overturning strength via the results of section 3. The key buoyancy variable that is affected by salinity is Δb_P, the difference between the northern and southern surface buoyancy maxima. Overturning strength is sensitive to Δb_S as well, but Δb_S does not vary much for a wide range of Q_S largely because surface salinity in the deep-water formation region does not vary much. Moreover, surface temperature is strongly controlled by the boundary condition and not greatly affected by Q_S, so Δb_P should be related to the salinity field by

$$\Delta b_P = (\beta g/\rho_0)(\Delta S_N - \Delta S_S) = (\beta g/\rho_0)\Delta S_P. \quad (17)$$

For most runs with default (30 day) temperature restoring strength, this is indeed a good approximation, with the estimate generally 70%–90% of the actual value. There are actually two significant corrections to (17), but the corrections tend to cancel each other out. The subordinate hemisphere maximum surface buoyancy does not occur at the polar boundary; the salinity is too low there, so the buoyancy maximum is pushed equatorward where the water is saltier (raising Δb_P) and warmer (lowering Δb_P).

The northern hemisphere salinity range, ΔS_N, is estimated in the preceding section. There is a relatively large gyre contribution to the meridional salt transport in the southern hemisphere (figure not shown), which makes it difficult to estimate ΔS_S, the southern hemisphere range. However, because ΔS_S is small, a very rough estimate may be good enough, so we ignore all but the overturning component in (13). The meridional volume transport at 32°S is fed by three times the upwelling area that feeds the transport at 32°N, so (13) implies that $\Delta S_S \approx (\frac{1}{3})\Delta S_N$. This prediction is approximately true for all the experiments except for the slightly asymmetric state runs. Thus Δb_P can be predicted from first principles.

Section 3 showed that for a density profile similar to the mixed boundary condition experiments, $\Phi_{\pm}/\Phi_0$ is given by (12), with $\Phi_0 \propto \Delta b_S^{1/3}$. When modeled zonal-mean buoyancy differences are used, this rule is followed very closely by the $\Delta T = 30$°C experiments but only roughly by the high κ_H and $\Delta T = 3$°C experiments (Fig. 11). We were not able to determine why the prediction is better for $\Delta T = 30$°C than for the other experiments. Profiles of surface zonal average buoyancy for $\Delta T = 30$°C series do not look more like the temperature-only profiles than the other series. Section 3b showed that the relationship between 2H and 1H experiments should be the same for a wide variety of Δb_S, so the $\Delta T = 3$°C experiments should be no different than the $\Delta T = 30$°C experiments.

The heat transport in the mixed-boundary-condition experiments is quite similar to that in the temperature-

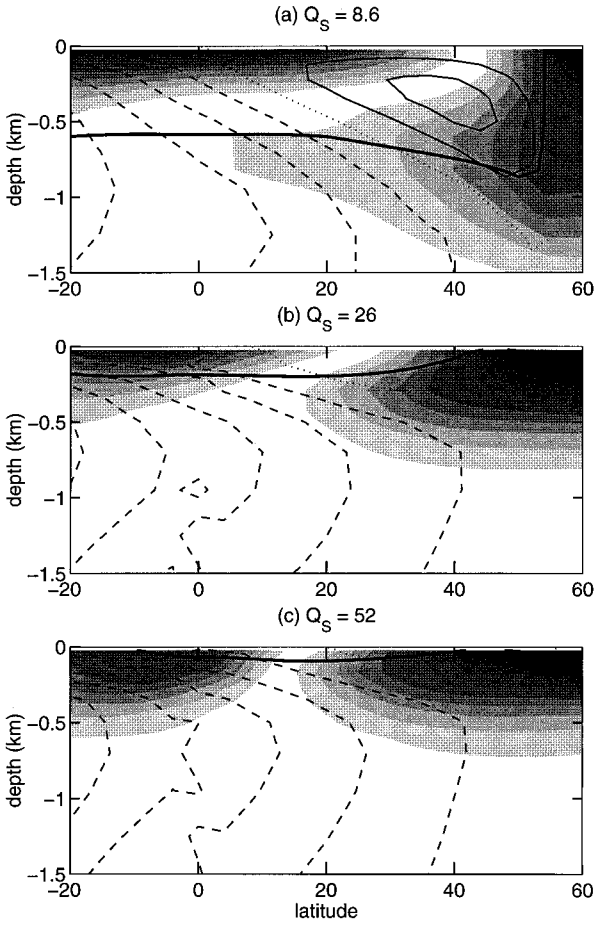

FIG. 12. Zonal average salinity (shaded), overturning streamfunction (thin contours), and densest isopycnal to outcrop at the surface in subordinate hemisphere (thick contours) for $\Delta T = 30$°C experiments with (a) $Q_S = 8.6$, (b) $Q_S = 26$, and (c) $Q_S = 52$. For each experiment, salinity contour interval is 1/20 of salinity range of the experiment. Darker shading represents fresher water in tongue protruding from northern boundary, but saltier water in tropical surface patch. Streamfunction contour interval is 2 Sv, with negative values dashed and zero contour dotted.

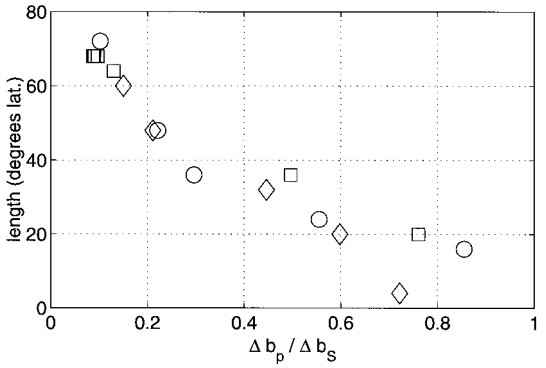

FIG. 13. Length of low salinity tongue (in degrees latitude) as a function of ratio of polar buoyancy difference to dominant hemisphere buoyancy range, for $\Delta T = 3$°C runs (circles), $\Delta T = 30$°C, default and high κ_H runs (squares and diamonds, respectively).

only experiments (Fig. 4). The temperature-only experiments impose a strong asymmetry between northern and southern hemisphere temperatures, whereas the temperature in mixed-boundary-condition experiments is approximately symmetrical about the equator. However, the thermocline in the dominant hemisphere and in much of the subordinate hemisphere does look similar in temperature-only and mixed-boundary-condition experiments. Thus the more idealized experiments capture the behavior of the more complicated experiments. The mixed-boundary-condition runs have somewhat smaller heat transports at the equator and in the dominant hemisphere because they have a larger gyre component opposing the overturning component.

3) LOW SALINITY TONGUE

In the asymmetric state, a subsurface tongue of low salinity water extends southward of its surface source (Fig. 12); in some cases the subsurface minimum extends for thousand of kilometers. This fresh tongue is reminiscent of the salinity signal associated with Antarctic Intermediate Water in the South Atlantic.

The low salinity tongue appears to be governed by a balance between southward advection of deep, low salinity from the northern boundary and downward diffusion of high salinity from the surface. The low salinity signal is injected below the surface by convection in the downward limb of the subordinate cell. This can be seen by comparing the maximum depth of the northern mixed layer and the mean depth of the fresh tongue in Fig. 12; the salinity signal reaches somewhat deeper than the mixed layer depth due to diffusion. When the subordinate-cell maximum density is nearly as great as the dominant-cell maximum density, the low salinity anomaly is relatively deep. In this case, it can travel for a relatively long distance before it is eroded by high salinity diffusing from above (Fig. 12a). Progressively shallower salinity injection results in progressively less prominant fresh tongues (Figs. 12b,c). These ideas are demonstrated by Fig. 13: the fresh tongue reaches farther as the density difference between the two polar boundaries decreases. The length of the tongue is defined here as the latitude range over which there is a subsurface minimum in the zonal average salinity. The buoyancy ranges are defined in terms of zonal average surface values; Δb_P is the difference between the southern hemisphere and northern hemisphere maxima, whereas Δb_S is the difference between the southern hemisphere maximum and the basin-wide minimum.

It is interesting that for the same $\Delta b_P/\Delta b_S$, the fresh tongue extends about equally far for experiments with $\Delta T = 30$°C, $\Delta T = 3$°C, and high κ_H. For the same $\Delta b_P/\Delta b_S$, the salinity minimum penetrates more deeply in the $\Delta T = 3$°C experiments than in the $\Delta T = 30$° experiments. However, the vertical advective-diffusive balance is also different in the two series, so that high surface salinity also diffuses to a greater depth in the

$\Delta T = 3°C$ experiments; apparently the two effects are equally strong. The result is insensitive to κ_H because the horizontal salinity transport is dominated by advection.

5. Conclusions

In a system driven by mixed boundary conditions, a hallmark of equatorially asymmetric circulation is the different roles played by temperature and salinity. One hemisphere, which we call the ''dominant'' hemisphere, has the strongest meridional circulation, minimizing the exposure of surface water to the surface fluxes of salinity (or, more realistically, of freshwater) at any particular latitude. This hemisphere is thus dominated by temperature forcing, and contains the densest surface water, which then forms the deep water for the entire system. The other, subordinate hemisphere is marked by slower circulation and hence greater sensitivity to the salinity forcing. Here, no surface water is dense enough to penetrate to the bottom, but the local density maximum produces intermediate water that drives a relatively shallow overturning cell. To summarize, the buoyancy range of the entire system is largely controlled by the imposed temperature range ΔT, while the degree of asymmetry is controlled by both ΔT and the salinity flux scale Q_S.

Experiments with surface buoyancy directly controlled through a restoring boundary condition show how meridional overturning cell transports of mass and heat depend on the surface buoyancy range in each hemisphere. Even a small asymmetry in surface buoyancy makes one overturning cell much stronger than the other, with a strong volume transport forced to cross the equator. A much greater buoyancy asymmetry does not produce a much greater circulation asymmetry. In the mixed boundary system, therefore, deep-water formation rate and cross-equatorial flow are primarily governed by ΔT. As long as Q_S is in the range that permits asymmetric flow, Q_S will have a smaller influence on the dominant cell strength. The subordinate cell strength Φ_- is more sensitive to Δb_P, the difference between the surface buoyancy maxima in the two hemispheres, so Φ_- does depend on Q_S. The subordinate cell is likely to be strongly influenced by wind stress, which is not included in this model, but the deepening of the subordinate cell with decreasing Δb_P, and hence with decreasing Q_S, should be a robust result. This deepening also deepens (and hence cools) the warm limb of the cross-equatorial circulation so that Q_S has a significant influence on cross-equatorial heat transport.

A two-hemisphere basin with strongly asymmetric circulation has a somewhat broader pycnocline, correspondingly weaker upwelling, and nearly double the meridional volume transport of a one-hemisphere basin with equivalent forcing. The differences can be accounted for by scalings based on the classical assumptions of large-scale geostrophy and vertical advective–diffusive balance. However, care must be taken to close the system of scale relations with the continuity equation rather than with the commonly applied linear vorticity relation. The latter equation does not include important contributions to vorticity in the western boundary current.

It is more difficult to explain quantitatively how overturning strength depends on Δb_P, but it is clear that the general pattern depends on the existence of a pycnocline. The total upwelling is controlled by diffusion in the pycnocline; the strengths of the two cells are largely determined by how they divide this fixed amount of upwelling. Even a modest Δb_P forces the relatively small subpycnocline range of buoyancy to be filled by the dominant cell. This gives the dominant cell access to at least the base of the pycnocline over most of basin so that it can grow strong at the expense of the subordinate cell.

The power law for overturning Φ found here appears to be more complicated than the linear relationships between flow strength and meridional density differences found in global GCMs (Hughes and Weaver 1994; Rahmstorf 1996). On closer inspection, however, we have shown that the Hughes and Weaver result is consistent with the classical scaling. This has implications in formulating box models, which for simplicity typically assume that Φ is proportional to Δb between boxes (e.g., Rooth 1982; Scott et al. 1999). The classical ⅓ power law is appropriate to surface buoyancy and the linear law is appropriate to a double vertical integral of density, but a box model should be based on a single vertical integral. In that case, the reasoning in section 3b yields $\Phi \propto \Delta b^{1/2}$.

In contrast to the Hughes and Weaver (1994) model, Rahmstorf (1996) pointed out that much of the North Atlantic Deep Water in his model did not upwell in the midlatitude Atlantic; hence, the Atlantic thermocline depth was unrelated to overturning strength. This significantly changed the scaling as expressed in (9), leading to linear dependence of overturning on meridional density differences. However, how global upwelling is distributed is still a somewhat open question. For instance, the horizontal (rather than isopycnal) eddy diffusivity commonly used in general circulation models may overstate the amount of upwelling in the Antarctic Circumpolar Current (Danabasoglu and McWilliams 1995).

The approximate surface distribution of salinity, and hence of density, can be related to Q_S and ΔT via approximations for the meridional salt transport. Our approximation is fairly crude since it does not take into account the effects of Q_S on the circulation, such as the existence of the subordinate cell. It can be thought of as essentially a box model, with the attributes more closely attuned to the dynamics of three-dimensional circulations than in previous work, such as Rooth (1982) or Thual and McWilliams (1992). In the more sensitive subordinate hemisphere, the salt transport is dominated

by zonal-average (hence two-dimensional) properties such as meridional overturning. However, the strength of these processes is different for two- and three-dimensional systems. The degree of asymmetry of the system can be described by the relative salinity range $s = \beta\Delta S/\alpha\Delta T$, where ΔS is the salinity contrast in the subordinate hemisphere and α and β are the thermal and haline expansion coefficients, respectively. Here, s measures the relative contribution of salinity to density variations; for the three-dimensional system, s is constant along curves of $Q_S \propto \Delta T^{4/3}$.

The system appears to be governed by a ''subcritical pitchfork bifurcation,'' in which both symmetric and asymmetric solutions can coexist for the same parameters. This is consistent with the two-dimensional results of Dijkstra and Molemaker (1997), in which the nature of the bifurcation depends on details of the surface forcing. Horizontal diffusivity raises the value of the minimum Q_S for which the asymmetric state exists and is stable. This is also consistent with two-dimensional results (Thual and McWilliams 1992) and suggests that the minimum Q_S rises when wind forcing is added to the thermohaline circulation. The location of the regime boundaries must be viewed with some caution because, in reality, the ocean is coupled to an atmosphere in which meridional transports of heat and moisture can affect the stability of a state (Nakamura et al. 1994; Saravanan and McWilliams 1995; Marotzke 1996). We show that capturing the atmospheric temperature feedback by weakening the surface temperature constraint raises the minimum Q_S for which a stable asymmetric state exists. However, a two-dimensional model shows that such a configuration is more unstable than a coupled model, in which moisture feedbacks are also included (Capotondi and Saravanan 1996).

It is not clear how many asymmetric steady states are possible for a given set of parameters. We stumbled upon at least three stable equilibria for $\Delta T = 3$°C, with significant basinwide changes in overturning strength and T–S–ρ characteristics. However, we could not find multiple asymmetric states for the more realistic $\Delta T = 30$°C. Dijkstra and Molemaker (1997) also show a hint of multiple asymmetric states (their Figs. 15 and 16). We attempted to construct a box model that included some of the subtleties of the relationships among salinity, overturning strength, and meridional salt transport. None of our attempts produced the multiple states seen here, nor did they display the vanishing of the asymmetric state at low Q_S described above, so we do not describe the model details in this paper.

The differences in circulation in our multiple states are larger than those between multiple convection states found by Lenderink and Haarsma (1994) in a three-level three-dimensional model, so purely local processes are unlikely to be responsible. If the real ocean displays such a multiplicity of states, it would indicate that significant changes in the global circulation could be forced by temporary climate events. The existence of such states would imply a much richer range of responses for the thermohaline circulation, which is usually portrayed as choosing between convection or no-convection states for various oceans (Marotzke and Willebrand 1991) or ocean regions (Hughes and Weaver 1994).

The system studied here is rather idealized, though it does capture such Atlantic features as the north–south asymmetry in polar salinity, the concomitant dominance of one hemisphere over the other in deep-water production, and the tongue of low-salinity intermediate water (AAIW in the Atlantic) produced by the fresher hemisphere. The usefulness of such an idealization lies partly in the simplicity of the salt transport, which allows for a rough prediction of circulation properties from external parameters. The system also shows that the qualitative behavior illustrated by two-dimensional models holds for three-dimensional dynamics. An obvious next step would be to include more realistic features from the real world, building on the more idealized results to derive the rules governing the more complicated system. Prominent ''complications'' include the wind-driven gyres, nonlinearity in the equation of state, and the Antarctic Circumpolar Current.

Acknowledgments. Work on this paper was done under NSF Grant OCE-9521138. Financial support for JM was granted by the Tokyo Electric Power Company through the TEPCO/MIT Environmental Research Program. Kevin Kohler provided programming assistance. Thanks go to Andrew Weaver and Michael Eby for donating their flux-corrected transport code and for their help in using it, and to Ron Pacanowski and Stephen Griffies for assistance with MOM 2. We acknowledge Claes Rooth and Steve Meacham for many interesting and useful discussions about thermohaline circulation and the mathematics of bifurcations, Jeff Scott, Thomas Stocker, and two anonymous reviewers for extensive suggestions, and Bob Hallberg for his comments.

REFERENCES

Arakawa, A., and V. Lamb, 1977: Computational design of the basic dynamical processes of the UCLA general circulation model. *Meth. Comput. Phys.* **17,** 174–267.

Armi, L., 1978: Some evidence for boundary mixing in the deep ocean. *J. Geophys. Res.*, **83,** 1971–1979.

Böning, C. W., W. R. Holland, F. O. Bryan, G. Danabasoglu, and J. C. McWilliams, 1995: An overlooked problem in model simulations of the thermohaline circulation and heat transport in the Atlantic Ocean. *J. Climate,* **8,** 515–523.

Bryan, F., 1986: High-latitude salinity effects and interhemispheric thermohaline circulation. *Nature,* **323,** 301–304.

——, 1987: Parameter sensitivity of primitive equation ocean general circulation models. *J. Phys. Oceanogr.,* **17,** 970–985.

Bryan, K., 1984: Accelerating the convergence to equilibrium of ocean-climate models. *J. Phys. Oceanogr.,* **14,** 666–673.

——, and M. D. Cox, 1967: A numerical investigation of the oceanic general circulation. *Tellus,* **19,** 54–80.

Capotondi, A., and R. Saravanan, 1996: Sensitivity of the thermohaline circulation to surface buoyancy forcing in a two-dimensional ocean model. *J. Phys. Oceanogr.,* **26,** 1039–1058.

Cessi, P., and W. Young, 1992: Multiple equilibria in two-dimensional thermohaline circulation. *J. Fluid Mech.,* **241,** 291–309.
Colin de Verdiere, A., 1988: Buoyancy driven planetary flows. *J. Mar. Res.,* **46,** 215–265.
Cox, M. D., 1984: A primitive equation, 3-dimensional model of the ocean. GFDL Ocean Group Tech. Rep. 1, Geophysical Fluid Dynamics Laboratory/NOAA, 40 pp. [Available from GFDL/NOAA, Princeton University, P.O. Box 308, Princeton, NJ 08542.]
——, 1989: An idealized model of the World Ocean. Part I: The global-scale water masses. *J. Phys. Oceanogr.,* **19,** 1730–1752.
Danabasoglu, G., and J. C. McWilliams, 1995: Sensitivity of the global ocean circulation to parameterization of mesoscale tracer transports. *J. Climate,* **8,** 2967–2987.
——, ——, and P. R. Gent, 1994: The role of mesoscale tracer transports in the global ocean circulation. *Science,* **264,** 1123–1126.
Dijkstra, H. A., and M. J. Molemaker, 1997: Symmetry breaking and overturning oscillations in thermohaline-driven flows. *J. Fluid Mech.,* **331,** 169–198.
Drazin, P. G., 1992: *Nonlinear Systems.* Cambridge University Press, 317 pp.
England, M. H., 1993: Representing the global-scale water masses in ocean general circulation models. *J. Phys. Oceanogr.,* **23,** 1523–1552.
Gargett, A. E., and G. Holloway, 1992: Sensitivity of the GFDL ocean model to different diffusivities for heat and salt. *J. Phys. Oceanogr.,* **22,** 1158–1177.
Gent, P. R., and J. C. McWilliams, 1990: Isopycnal mixing in ocean circulation models. *J. Phys. Oceanogr.,* **20,** 150–155.
——, J. Willebrand, T. J. McDougall, and J. C. McWilliams, 1995: Parameterizing eddy-induced tracer transports in ocean circulation models. *J. Phys. Oceanogr.,* **25,** 463–474.
Gordon, A. L., 1986: Interocean exchange of thermocline water. *J. Geophys. Res.,* **91,** 5037–5046.
Huang, R. X., 1994: Thermohaline circulation: Energetics and variability in a single-hemisphere basin model. *J. Geophys. Res.,* **99,** 12 471–12 485.
——, and R. L. Chou, 1994: Parameter sensitivity study of the saline circulation. *Climate Dyn.,* **9,** 391–409.
Hughes, T. C. M., and A. J. Weaver, 1994: Multiple equilibria of an asymmetric two-basin ocean model. *J. Phys. Oceanogr.,* **24,** 619–637.
Ledwell, J. R., and A. Bratkovich, 1995: A tracer study of mixing in the Santa Cruz Basin. *J. Geophys. Res.,* **100,** 20 681–20 704.
Lenderink, G., and R. J. Haarsma, 1994: Variability and multiple equilibria of the thermohaline circulation associated with deep-water formation. *J. Phys. Oceanogr.,* **24,** 1480–1493.
Levitus, S., and T. P. Boyer, 1994: *World Ocean Atlas 1994,* Vol. 4: *Temperature.* NOAA Atlas NESDIS 4, NOAA, NESDIS, Washington, DC, 117 pp.
Macdonald, A. M., 1993: Property fluxes at 30° S and their implications for the Pacific–Indian Throughflow and the global heat budget. *J. Geophys. Res.,* **98,** 6851–6868.
——, and C. Wunsch, 1996: An estimate of global ocean circulation and heat fluxes. *Nature,* **382,** 436–439.
Marotzke, J., 1990: Instabilities and multiple equilibria of the thermohaline circulation. Ph.D. thesis, Berichte Institut für Meereskunde, Kiel, Germany, 126 pp. [Available from J. Marotzke, Center for Global Change Science, MIT, Rm. 54-1514, Cambridge, MA 02139.]
——, 1996: Analysis of thermohaline feedbacks. *Decadal Climate Variability: Dynamics and Predictability.* D. L. T. Anderson and J. Willebrand, Eds., NATO ASI Series, 333–378.
——, 1997: Boundary mixing and the dynamics of three-dimensional thermohaline circulations. *J. Phys. Oceanogr.,* **27,** 1713–1728.
——, and J. Willebrand, 1991: Multiple equilibria of the global thermohaline circulation. *J. Phys. Oceanogr.,* **21,** 1372–1385.
——, and D. W. Pierce, 1997: On spatial scales and lifetimes of SST anomalies beneath a diffusive atmosphere. *J. Phys. Oceanogr.,* **27,** 133–139.
——, P. Welander, and J. Willebrand, 1988: Instability and multiple steady states in a meridional-plane model of the thermohaline circulation. *Tellus,* **40A,** 162–172.
Mikolajewicz, U., and E. Maier-Reimer, 1994: Mixed boundary conditions in ocean general circulation models and their influence of the stability of the model's conveyor belt. *J. Geophys. Res.,* **99,** 22 633–22 644.
Munk, W., 1966: Abyssal recipes. *Deep-Sea Res.,* **13,** 707–730.
Nakamura, M., P. H. Stone, and J. Marotzke, 1994: Destabilization of the thermohaline circulation by atmospheric eddy transports. *J. Climate,* **7,** 1870–1882.
Pacanowski, R. C., 1996: MOM 2 documentation, user's guide and reference manual. GFDL Ocean Tech. Rep. 3.1, Geophysical Fluid Dynamics Laboratory/NOAA, Princeton, NJ. [Available from GFDL/NOAA, Princeton University, P.O. Box 308, Princeton, NJ 08542.]
Peixoto, J. P., and A. H. Oort, 1992: *Physics of Climate.* Amer. Inst. Phys., 520 pp.
Peterson, W. H., 1979: A steady thermohaline convection model (driven by turbulent buoyant plumes from multiple isolated sources in a large non-turbulent finite region, with applications to the oceanic thermocline circulation). Ph.D. thesis, University of Miami, 160 pp.
Quon, C., and M. Ghil, 1992: Multiple equilibria in thermosolutal convection due to salt-flux boundary conditions. *J. Fluid Mech.,* **245,** 449–483.
——, and ——, 1995: Multiple equilibria and stable oscillations in the thermosolutal convection at small aspect ratio. *J. Fluid Mech.,* **291,** 33–56.
Rahmstorf, S., 1996: On the freshwater forcing and transport of the Atlantic thermohaline circulation. *Climate Dyn.,* **12,** 799–811.
——, and J. Willebrand, 1995: The role of temperature feedback in stabilising the thermohaline circulation. *J. Phys. Oceanogr.,* **25,** 787–805.
Rintoul, S. R., 1991: South Atlantic interbasin exchange. *J. Geophys. Res.,* **96,** 2675–2692.
Rooth, C., 1982: Hydrology and ocean circulation. *Progress in Oceanography,* Vol. 11, Pergamon, 131–149.
Saravanan, R., and J. C. McWilliams, 1995: Multiple equilibria, natural variability, and climate transitions in an idealized ocean–atmosphere model. *J. Climate,* **8,** 2296–2323.
Schmidt, G. A., and L. A. Mysak, 1996: The stability of a zonally averaged thermohaline circulation model. *Tellus,* **48,** 158–178.
Schmitt, R. W., P. S. Bogden, and C. E. Dorman, 1989: Evaporation minus precipitation and density fluxes for the North Atlantic. *J. Phys. Oceanogr.,* **19,** 1208–1221.
Scott, J. R., J. Marotzke, and P. H. Stone, 1999: Interhemispheric thermohaline circulation in a coupled box model. *J. Phys. Oceanogr.,* **29,** 351–365.
Speer, K. G., and M. S. McCartney, 1991: Tracing lower North Atlantic Deep Water across the equator. *J. Geophys. Res.,* **96,** 20 443–20 448.
Stocker, T. F., and D. G. Wright, 1991: A zonally averaged ocean model for the thermohaline circulation. Part II: Interocean circulation in the Pacific–Atlantic basin system. *J. Phys. Oceanogr.,* **21,** 1725–1739.
——, D. G. Wright, and L. A. Mysak, 1992: A zonally averaged, coupled ocean–atmosphere model for paleoclimate studies. *J. Climate,* **5,** 773–797.
Stommel, H., 1961: Thermohaline convection with two stable regimes of flow. *Tellus,* **13,** 224–230.
——, and A. B. Arons, 1960: On the abyssal circulation of the World Ocean. Part I: Stationary planetary flow patterns on a sphere. *Deep-Sea Res.,* **6,** 140–154.
——, ——, and A. J. Faller, 1958: Some examples of stationary planetary flow patterns in bounded basins. *Tellus,* **10,** 179–187.
Thual, O., and J. C. McWilliams, 1992: The catastrophe structure of thermohaline convection in a two-dimensional fluid model and a comparison with low-order box models. *Geophys. Astrophys. Fluid Dyn.,* **64,** 67–95.

Toole, J. M., R. W. Schmitt, K. L. Polzin, and E. Kunze, 1997: Near-boundary mixing above the flanks of a midlatitude seamount. *J. Geophys. Res.,* **102,** 947–959.

Tziperman, E., 1997: Inherently unstable climate behavior due to weak thermohaline ocean circulation. *Nature,* **386,** 592–595.

Vellinga, M., 1996: Instability of two-dimensional thermohaline circulation. *J. Phys. Oceanogr.,* **26,** 305–319.

Veronis, G., 1975: The role of models in tracer studies. *Numerical Models of the Ocean Circlation,* U.S. Natl. Acad. Sci., 133–145.

Wang, X., P. H. Stone, and J. Marotzke, 1999a: Global thermohaline circulation. Part I: Sensitivity to Atmospheric Moisture Transport. *J. Climate,* **12,** 71–82.

——, ——, and ——, 1999b: Global thermohaline circulation. Part II: Sensitivity with interactive atmospheric transports. *J. Climate,* **12,** 83–91.

Warren, B. A., 1981: Deep circulation of the World Ocean. *Evolution of Physical Oceanography,* B. A. Warren and C. Wunsch, Eds., MIT Press, 6–42.

——, 1983: Why is no deep water formed in the North Pacific? *J. Mar. Res.,* **41,** 327–347.

Weaver, A. J., and E. S. Sarachik, 1990: On the importance of vertical resolution in certain ocean general circulation models. *J. Phys. Oceanogr.,* **20,** 600–609.

——, and ——, 1991: The role of mixed boundary conditions in numerical models of the ocean's climate. *J. Phys. Oceanogr.,* **21,** 1470–1493.

——, and M. Eby, 1997: On the numerical implementation of advection schemes for use in conjunction with various mixing parameterizations in the GFDL ocean model. *J. Phys. Oceanogr.,* **27,** 369–377.

——, E. S. Sarachik, and J. Marotzke, 1991: Freshwater flux forcing of decadal and interdecadal oceanic variability. *Nature,* **353,** 836–838.

——, J. Marotzke, P. F. Cummins, and E. S. Sarachik, 1993: Stability and variability of the thermohaline circulation. *J. Phys. Oceanogr.,* **23,** 39–60.

Weber, S. L., 1998: Parameter sensitivity of a coupled atmosphere–ocean model. *Climate Dyn.,* **14,** 201–212.

Welander, P., 1986: Thermohaline effects in the ocean circulation and related simple models. *Large-Scale Transport Processes in Oceans and Atmospheres,* J. Willebrand and D. L. T. Anderson, Eds., NATO ASI Series, D. Reidel, 163–200.

Wijffels, S. E., R. W. Schmitt, H. L. Bryden, and A. Stigebrandt, 1992: Transport of freshwater by the oceans. *J. Phys. Oceanogr.,* **22,** 155–162.

Winton, M., 1996: The role of horizontal boundaries in parameter sensitivity and decadal-scale variability of coarse-resolution ocean general circulation models. *J. Phys. Oceanogr.,* **26,** 289–304.

——, and E. S. Sarachik, 1993: Thermohaline oscillations induced by strong steady salinity forcing of ocean general circulation models. *J. Phys. Oceanogr.,* **23,** 1389–1410.

Wunsch, C., 1970: On oceanic boundary mixing. *Deep-Sea Res.,* **17,** 293–301.

Zhang, J., R. W. Schmitt, and R. X. Huang, 1998: Sensitivity of GFDL Modular Ocean Model to the parameterization of double-diffusive processes. *J. Phys. Oceanogr.,* **28,** 589–605.